Chapter 3
Stochastic Effects in Quorum Sensing

Marc Weber and Javier Buceta

3.1 Introduction

All of us have surely played the "broken telephone." In that game a group of people arrange in a circle and one participant passes a message to one of his/her neighbors. The message is whispered/mumbled, such that it is difficult to understand, and passed progressively along the participants until it reaches the original messenger. The funny part of the game consists in comparing the original message and the one that finally arrives (normally they have nothing to do with each other!). The "broken telephone" nicely illustrates how noise interferes with the signal in communication processes. Since quorum sensing (QS) is nothing but that, a communication mechanism, one may wonder how noise interferes with it, how bacteria cope with fluctuations, and how to provide a modeling framework for addressing these questions.

Yet, what do we mean by noise? Over the past decade a number of studies have shown that the level and activity of the species involved in gene regulatory circuits fluctuate [1]. While extrinsic factors are in some cases the source of these fluctuations (e.g., light fluctuations in circadian clocks [2]), in most situations they are mainly due to the inherent randomness of biochemical reactions when the number of molecules is very low [3]. Under these conditions, the value of the mean and the variance are of the same order and consequently the deterministic description fails. Notably, biochemical noise, either intrinsic or extrinsic, is not

M. Weber
Co.S.Mo. Lab (Computer Simulation and Modeling), Parc Cientific de Barcelona, C/Baldiri Reixac 4-8, Barcelona 08028, Spain

J. Buceta (✉)
Department of Chemical and Biomolecular Engineering, Lehigh University, 111 Research Drive, Room D316 Bethlehem, PA 18015, USA
e-mail: jbuceta@gmail.com

S.J. Hagen (ed.), *The Physical Basis of Bacterial Quorum Communication*, Biological and Medical Physics, Biomedical Engineering, DOI 10.1007/978-1-4939-1402-9_3

necessarily a nuisance but a biological component that is essential and has a positive functional role in many situations [4]: for example, improving cellular regulation [5].

In the particular case of QS, the detection of the freely diffusing signaling molecule, the autoinducer, is subject to intense molecular noise [6]. Still, QS bacteria cope with these fluctuations reliably. For example, the typical volume of *Vibrio fischeri* bacteria is $0.35\,\mu m^3$, and a concentration of 10 nM of autoinducer already induces a QS response [7]. This means that just $\sim$2 signaling molecules per cell are enough to be sensed by this small marine bacterium. The low number of signaling molecules inside the cell, together with the other possible sources of noise, indicates that the fluctuations at the autoinducer level must be taken under consideration for a deep understanding of the QS pathway activation and functioning. Moreover, the stochastic effects in QS pose the intriguing question of how cells achieve a coordinated response in the presence of noise. Indeed, the QS mechanism may produce a robust and synchronized behavior at the level of the population [8]. However, how this behavior at the collective level arises from the stochastic dynamics of individual cells is puzzling. At the end, a collective response means a precise information exchange in the colony: the quantification of the number of cells, the density, in the colony. Consequently, how can a bacterial population estimate its number of constituents precisely if such information is fuzzy at the single cell level?

At the most fundamental level, cell communication by QS relies on the diffusion of a signaling molecule through the cell membrane. Recent studies have shown that diffusion reduces the noise at the level of the autoinducer [9]; however, the interplay between the diffusion process and some standard sources of stochasticity (transcriptional and biochemical noise) has remained elusive until very recently [10]. Moreover, while in eukaryotes the diffusion seems to contribute for enhancing the precision of regulatory processes [11], similar effects have not been reported in the context of QS. Thus, a first central question is to elucidate how the diffusion process influences, and interplay with, the fluctuations in the signaling molecule.

Another relevant point refers to the relation between the QS signaling network architecture and its ability to filter and/or enhance and/or suppress noise. While this question is case dependent, general clues and answers can be obtained by studying simple QS systems, e.g. the LuxI/LuxR system, as the underlying signaling motif in most QS species is a positive feedback loop leading to phenotypic bistability [12]. As a matter of fact, a number of studies have shown that noise plays an important role in bistable systems [13–17]. In the context of QS, it has been recently revealed how noise at different levels of the signaling network controls the precision of the collective response [18] and, ultimately, how noise modifies the phenotypic landscape that produces the observed heterogeneity in QS colonies.

Herein we shed light on these aspects of the stochasticity in QS communication by reviewing recent advances in the field. Altogether, the results suggest that bacteria have adapted their communication mechanisms in order to improve the signal-to-noise ratio and to adjust the intensity of the fluctuations depending on the environmental conditions. The chapter is organized as follows. We first illustrate by

means of a toy model how, at the onset of the QS transition, the autoinducer diffusion process conditions the QS dynamics and that the interplay between different sources of noise establishes ranges of diffusion values that minimize the noise at the autoinducer level. We then show by means of a detailed model of the LuxI/LuxR system how fluctuations interfere with the synchronization of the cell activation process and lead to a bimodal phenotypic distribution. In this context, we review the concept of precision in order to characterize the reliability of the QS communication process in the colony. In terms of the network architecture, we show that increasing the noise in the expression of LuxR helps cells to get activated at lower autoinducer concentrations but, at the same time, slows down the global response. Some of the observed properties are rather counterintuitive, e.g. noise at the level of LuxR helps cell to become activated at low autoinducer values but above a certain threshold of the autoinducer concentration the fluctuations stabilize the cell at the unactivated phenotype. As we will see, the latter can be explained by analyzing how noise modifies the phenotypic landscape. Finally, we present the main conclusions and discuss the applicability and relevance of these studies in the context of noise in QS communication.

3.2 Diffusion and Noise

QS communication relies on the diffusion of the signaling molecule through the cell membrane. On top of that, the autoinducer is subjected to different sources of noise and the following question naturally arises: what is the interplay between the diffusion process and the autoinducer stochastic dynamics? In this regard, a recent study has shown that diffusion, together with a fast turnover of the QS transcriptional regulator, attenuates low-frequency components of extrinsic noise at the level of the autoinducer [9]. These authors have coined the term “diffusional dissipation” that emphasizes the importance of fast signal turnover (or dissipation) by diffusion in QS. Other studies have used some characteristics of the diffusion process in Gram-negative bacteria (the permeability of the cell membrane to the autoinducer and the symmetry of autoinducer diffusion) to demonstrate that the extracellular noise is required for a stable synchronization in the colony [19].

These studies assume a constitutive expression of the QS master regulators. However, QS communication also relies on situations when the levels of transcription/translation are very low and the system lacks autoinduction. Thus, at low cell density, *luxI* gene expression is either repressed by a high concentration of its repressor or activated at a very low level by its activator. Under these conditions, very few *luxI* transcripts are produced and the feedback regulation of the *luxI* gene leading to autoinduction can be disregarded. Such infrequent transcription events have been observed in many bacterial operons. For example, single molecule experiments have shown that the infrequent dissociation of the lac repressor produces rare transcription events leading to just one mRNA molecule [20, 21]. Importantly, when the transcription rate is very low, the so-called transcriptional noise is a major source of stochasticity [3].

In this section we focus on the interplay between the diffusion process and the transcriptional and intrinsic noises. We aim at understanding how the communication mechanism and different sources of noise determine the dynamics of the autoinducer. We restrict ourselves to the study of the aforementioned problems below the QS activation threshold where we can assume that the transcription events produce basal constitutive levels of mRNA of at most one molecule per cell at a time and the regulatory feedback loop can be neglected.

3.2.1 Modeling the LuxI mRNA Leaky Dynamics

Below the activation (autoinduction) threshold, it can be assumed that rare (basal) transcription events produce individual *luxI* transcripts. Under these conditions the dynamics of the mRNA can be then described by means of a Markovian dichotomous process [22],

$$M_0^i \underset{\alpha}{\overset{\beta}{\rightleftarrows}} M_1^i \tag{3.1}$$

where $M_{0,1}^i = 0, 1$ stands for the number of mRNA molecules at cell i and α and β for the transition rates between these states; i.e., α and β account for the mRNA degradation rate and the transcription frequency, respectively. Notice that the fluctuations of the mRNA dynamics are not memoryless, i.e. white. Once an mRNA molecule is produced, and until it becomes degraded, the cell keeps producing the autoinducer. That is, the transcriptional noise is a colored noise, and its autocorrelation decays exponentially with a characteristic time scale $\tau_c = (\alpha + \beta)^{-1}$ [22].

Once an mRNA molecule is produced it leads to the appearance of functional LuxI synthetases. It has been shown that the amount of the synthetase substrate is not a limiting factor for the production of the autoinducer [23, 24]. As a consequence, the levels of the signaling molecule depend directly on the expression levels of the synthetase. Ignoring intermediate biochemical steps in the autoinducer synthesis reduces the number of noise sources and may even change, under some circumstances, the observed dynamics [25]. Still, it is a valid approximation in most cases and one can assume that the translation of the synthetase and the subsequent synthesis of the autoinducer, A, can be effectively described by a single chemical step with rate k_+. In addition, the autoinducer becomes degraded at a rate k_-, that is,

$$M_1^i \xrightarrow{k_+} M_1^i + A^i \tag{3.2}$$

$$A^i \xrightarrow{k_-} \varnothing \tag{3.3}$$

$$A_{\text{ext}} \xrightarrow{k_-} \varnothing \ . \tag{3.4}$$

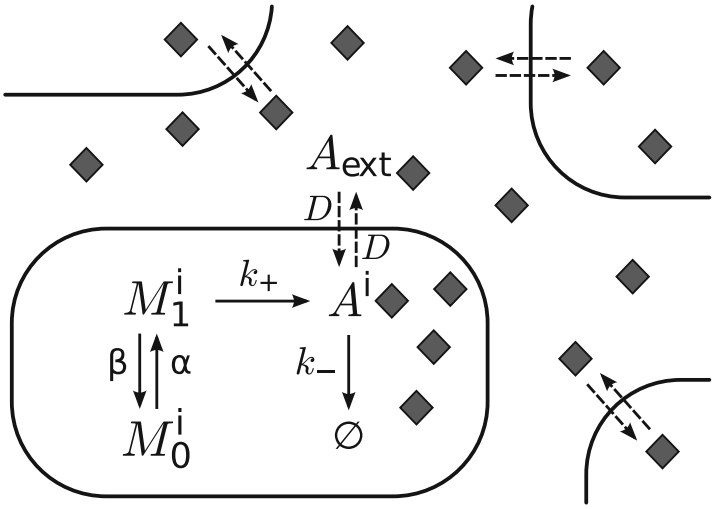

Fig. 3.1 Scheme of a simplified biochemical QS network near the activation threshold. Schematic representation of the biochemical processes considered for describing the dynamics of the signaling molecule, A (*diamonds*), in cell i. The mRNA dynamics follow a dichotomous process with state values $M_{0,1}$ corresponding to zero and one molecule, respectively. Once the autoinducer has been produced, it can diffuse into and out of the cell leading to cell communication

where A_{ext} accounts for the number of signaling molecules in the extracellular medium. Passive diffusion in and out the cell of the autoinducer can be implemented by means of the reaction:

$$A^i \underset{rD}{\overset{D}{\rightleftarrows}} A_{\text{ext}} \tag{3.5}$$

where D stands for the diffusion rate and $r = V/V_{\text{ext}}$ represents the ratio of the volume of a cell to the total extracellular volume. Figure 3.1 schematically represents the biochemical processes described by the set of reactions (3.1)–(3.5).

3.2.2 Null-intrinsic Noise Approximation

Two stochastic contributions drive the dynamics of A: the mRNA fluctuations due to the random switching and the intrinsic noise due to low copy number of the resulting autoinducer. As of the latter, it can be neglected if over the course of time $A^i/\left(A^i+1\right) \simeq 1$ ("large" number of autoinducer molecules). While such approximation is not justified (see parameters values below), it is useful to implement it in order to discriminate between the effects caused by different stochastic contributions and to obtain analytical expressions. In this case, it is

straightforward to demonstrate that the dynamics of the autoinducer, (3.1)–(3.5), can be described by the following coupled stochastic equations:

$$\dot{c}_{A^i} = k_+ c_{M_1^i}(t) - k_- c_{A^i} + D\left(c_{A_{\text{ext}}} - c_{A^i}\right) \tag{3.6}$$

$$\begin{aligned}\dot{c}_{A_{\text{ext}}} &= -k_- c_{A_{\text{ext}}} + rD\sum_{i=1}^{N}\left(c_{A^i} - c_{A_{\text{ext}}}\right) \\ &= -k_- c_{A_{\text{ext}}} + rDN\left(\langle c_A\rangle - c_{A_{\text{ext}}}\right),\end{aligned} \tag{3.7}$$

where $c_{A^i} = A^i/V$, $c_{M_1^i}(t) = M_1^i/V$, and $c_{A_{\text{ext}}} = A_{\text{ext}}/V_{\text{ext}}$ stand for the concentration of species A and M_1^i at cell i and for species A_{ext} at the extracellular medium, respectively, N is the bacterial colony size, and $\langle\cdot\rangle$ represents the population average. In Eq. (3.6) the term $c_{M_1^i}(t)$ accounts for a dichotomous stochastic process characterized by the rates and states (α, β) and $(0, 1/V)$, respectively, and describes the fluctuating dynamics of the mRNA concentration.

By implementing a quasi-steady approximation for the dynamics of the external autoinducer, i.e. $\dot{c}_{A_{\text{ext}}} = 0$ we obtain that,

$$c_{A_{\text{ext}}} = \langle c_A\rangle \frac{1}{1+\frac{k_-}{NDr}}\,. \tag{3.8}$$

By substituting (3.8) into (3.6) we obtain a rate equation for the concentration of the signaling molecule inside a given cell that depends on the average $\langle c_A\rangle$ (the index i has been dropped),

$$\dot{c}_A = k_+ c_{M_1}(t) - D\left(1+\frac{k_-}{D}\right)c_A + \langle c_A\rangle \frac{D}{1+\frac{k_-}{NDr}}\,. \tag{3.9}$$

In the absence of diffusion, Eq. (3.9) reveals that the concentration of the signaling molecule reaches a maximum value of $c_A^+ = k_+/(k_- V)$ when $c_{M_1}(t) = V^{-1}$. In terms of c_A^+ and the time scale $t_c = 1/k_-$ (the typical lifetime of a signaling molecule), the dimensionless version of (3.9) reads

$$\dot{\tilde{c}}_A = \hat{c}_{M_1}(\tilde{t}) + k_+^{\text{eff}}\left(\langle\tilde{c}_A\rangle\right) - k_-^{\text{eff}}\tilde{c}_A\,, \tag{3.10}$$

where

$$\tilde{D} = D/k_- \tag{3.11}$$

$$k_-^{\text{eff}} = 1 + \tilde{D} \tag{3.12}$$

$$k_+^{\text{eff}}\left(\langle\tilde{c}_A\rangle\right) = \langle\tilde{c}_A\rangle\,\frac{\tilde{D}}{1+\frac{1}{N\tilde{D}r}}\,; \tag{3.13}$$

$\hat{c}_{M_1}(\tilde{t})$ being a Markovian dichotomous noise with states $\{\hat{c}_{M_1}\} = 0, 1$ and rates $\tilde{\alpha} = \alpha/k_-$ and $\tilde{\beta} = \beta/k_-$. Equation (3.10) can be formally closed by invoking the following self-consistency condition:

$$\langle \tilde{c}_A \rangle = \int_{\tilde{\Omega}} \tilde{c}_A \, \rho\left(\tilde{c}_A; \langle \tilde{c}_A \rangle\right) \mathrm{d}\tilde{c}_A, \tag{3.14}$$

$\rho\left(\tilde{c}_A; \langle \tilde{c}_A \rangle\right)$ being the probability density solving (3.10) and $\tilde{\Omega}$ its support (see below) [22]:

$$\rho\left(\tilde{c}_A; \langle \tilde{c}_A \rangle\right) = \mathscr{N}\left(k_-^{\mathrm{eff}} \tilde{c}_A - k_+^{\mathrm{eff}}\left(\langle \tilde{c}_A \rangle\right)\right)^{\frac{\tilde{\beta}}{k^{\mathrm{eff}}} - 1} \tag{3.15}$$

$$\left(1 + k_+^{\mathrm{eff}}\left(\langle \tilde{c}_A \rangle\right) - k_-^{\mathrm{eff}} \tilde{c}_A\right)^{\frac{\tilde{\alpha}}{k^{\mathrm{eff}}} - 1}, \tag{3.16}$$

with

$$\mathscr{N} = \frac{\left(1 + \tilde{D}\right) \Gamma\left[\frac{\tilde{\alpha}+\tilde{\beta}}{1+\tilde{D}}\right]}{\Gamma\left[\frac{\tilde{\alpha}}{1+\tilde{D}}\right] \Gamma\left[\frac{\tilde{\beta}}{1+\tilde{D}}\right]} \tag{3.17}$$

being the normalization constant. The condition (3.14) can be exactly solved and leads to the following value for the average concentration of autoinducer:

$$\langle \tilde{c}_A \rangle = \frac{1 + \tilde{D} N r}{1 + \tilde{D} N r + \tilde{D}} \frac{\tilde{\beta}}{\tilde{\alpha} + \tilde{\beta}} = \frac{1 + \tilde{D} N r}{1 + \tilde{D} N r + \tilde{D}} \langle \tilde{c}_A \rangle|_{\tilde{D}=0} \tag{3.18}$$

where $\langle \tilde{c}_A \rangle|_{\tilde{D}=0} = \tilde{\beta}/\left(\tilde{\alpha} + \tilde{\beta}\right)$ is the average concentration of the signaling molecule in the absence of diffusion. For the sake of concision, on what follows we drop in the notation of $\rho\left(\tilde{c}_A; \langle \tilde{c}_A \rangle\right)$ the term $\langle \tilde{c}_A \rangle$ from the argument. Note that $\rho\left(\tilde{c}_A\right)$ has two states (barriers) that define its support. That is, the minimum and maximum values that the concentration of the autoinducer can reach as a function of the diffusion are:

$$\tilde{c}_A^- = \frac{\tilde{D}^2 N r}{(1 + \tilde{D})(1 + \tilde{D} + \tilde{D} N r)} \frac{\tilde{\beta}}{\tilde{\alpha} + \tilde{\beta}} \tag{3.19}$$

$$\tilde{c}_A^+ = \tilde{c}_A^- + \frac{1}{1 + \tilde{D}}. \tag{3.20}$$

Moreover, it is easy to prove that the probability density $\rho\left(\tilde{c}_A\right)$ shows a single extremum if

$$\tilde{\alpha}, \tilde{\beta} \lesssim k_-^{\mathrm{eff}}, \tag{3.21}$$

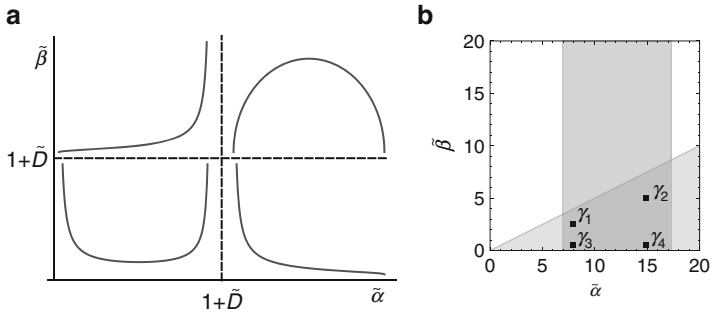

Fig. 3.2 Probability densities of the signaling molecule and parameter space. (**a**) Sketch of the different probability densities of the autoinducer concentration depending on the value of $\tilde{\alpha}$ and $\tilde{\beta}$ with respect to $\tilde{D}$. Given a set of values $(\tilde{\alpha}, \tilde{\beta})$ the dynamics of the autoinducer shows different behaviors depending on the value of the diffusion parameter since the transition lines are located at $\tilde{\alpha}, \tilde{\beta} = 1 + \tilde{D}$. The constraints set by the approach (one mRNA at a time) make the region on the top-left corner non-accessible. (**b**) Parameter space diagram $(\tilde{\alpha}, \tilde{\beta})$ indicating the sets of parameters used in simulations (*solid squares*): $\gamma_1 = (8, 2)$, $\gamma_2 = (15, 5)$, $\gamma_3 = (8, 0.5)$, $\gamma_4 = (15, 0.5)$. The experimental values reported for the degradation rate of the mRNA leads to a biological meaningful range for $\tilde{\alpha}$ (*rectangular region*). The low constitutive expression assumption is prescribed by the constraint $\tilde{\alpha} > 2\tilde{\beta}$ (*triangular region*)

where the extremum is a maximum if $\tilde{\alpha}, \tilde{\beta} > k_{-}^{\text{eff}}$ and a minimum if $\tilde{\alpha}, \tilde{\beta} < k_{-}^{\text{eff}}$. In other cases the probability density does not display any extrema. Therefore, as a function of $\tilde{\alpha}$ and $\tilde{\beta}$, the probability density $\rho(\tilde{c}_A)$ may show four different behaviors depending on the value of the diffusion coefficient as schematically represented in Fig. 3.2a. However, given the constraints on the parameters of our modeling not all regions, i.e. behaviors, are accessible to the autoinducer dynamics. In particular, we have assumed a low constitutive expression such that only a single mRNA molecule can be transcribed at a time. The latter implies that $\tilde{\beta} < \tilde{\alpha}$ (the degradation rate of the mRNA is larger than the transcription rate) in order to assure that a maximum of one mRNA molecule is present in a cell at any given time. As a consequence, and independently of the diffusion value, the dynamics leading to the probability density shown at the top-left region of Fig. 3.2a (for which $\tilde{\beta} > \tilde{\alpha}$) cannot be considered as physical in the context of a *luxI* leaky mRNA dynamics.

Finally, the noise of the autoinducer concentration can be estimated by computing the ratio between the variance and the mean[1]:

$$\eta^2_{\tilde{c}_A} = \frac{\sigma^2_{\tilde{c}_A}}{\langle \tilde{c}_A \rangle^2} = \frac{\tilde{\alpha}\left(1+\tilde{D}+\tilde{D}Nr\right)^2}{\tilde{\beta}\left(1+\tilde{D}\right)\left(1+\tilde{D}Nr\right)^2\left(1+\tilde{D}+\tilde{\alpha}+\tilde{\beta}\right)} \tag{3.22}$$

[1]Note that "noise" has been used with two different meanings: a stochastic contribution and, in this case, a quantity that effectively measures the effects of that stochastic contribution.

where $\sigma^2_{\tilde{c}_A} = \langle \tilde{c}_A^2 \rangle - \langle \tilde{c}_A \rangle^2$. Note that in a purely deterministic system $\eta^2_{\tilde{c}_A} = 0$. On the other hand, in systems where fluctuations play a relevant role in the dynamics $\eta^2_{\tilde{c}_A} \gtrsim 1$.

3.2.3 QS Switch at the Onset: Parameter Values

Herein we are particularly interested in the role played by the fluctuations of the signaling molecule, A, when its concentration is close, yet below, to the activation threshold of the QS switch such that autoinduction doesn't play a role and the basal leaky dynamics of the luxI mRNA holds. Therefore, we fix the mean concentration of the autoinducer and modulate the rest of the parameters in order to keep constant this value. According to some recent experiments [6], a value of $c_A^0 = 25$ nM is reasonable for most of the bacterial species when the value of the so-called sensing potential, $\nu = (rN)^{-1}$, is $\nu \sim 10^3$. In our simulations we choose $N = 10^2$ and then $V_{\text{ext}} = \nu N V = 10^5 V$ (i.e., $r = 10^{-5}$). Keeping ν to a constant value necessarily requires an external dilution protocol for maintaining constant the cell density and compensate for cell growth at a rate, $\sim 2 \cdot 10^{-2}$ min^{-1} (i.e., cell cycle duration $\sim$50 min). In addition, we notice that most autoinducer molecules are rather stable. For example, the degradation rate of the homoserine lactone 3-oxo-C6-AHL has been measured in vitro: $\sim 3 \cdot 10^{-4}$ min^{-1} [26]. The values in vivo has been also estimated [6]: $\sim 5 \cdot 10^{-3}$–$2 \cdot 10^{-2}$ min^{-1}. Consequently, the dilution process constitutes the main source of effective degradation of A, both inside and outside the cell.

As for the luxI mRNA dynamics, the half-lives of all mRNAs of *Staphylococcus aureus* have been recently measured during the mid-exponential phase. Most of the transcripts (90 %) have half-lives shorter than 5 min [27, 28]. According to these studies we restrict the mRNA degradation rate to the range $\ln(2)/5$ min^{-1} $< \alpha <$ $\ln(2)/2$ min^{-1} and consequently $\tilde{\alpha} > 1$. As for the frequency of the transcription events, β is determined by particular characteristics of the gene regulatory process under consideration, like the affinity of the regulatory proteins to the operator site and the initiation rate of transcription. Due to the assumption of low constitutive transcription, we choose values of parameter β satisfying the relation $\alpha > \beta$. In particular in our simulations we implement the more restrictive condition $\alpha > 2\beta$. Figure 3.2b recapitulates the different sets of α and β values that we use in our simulations and analytical calculations. Summarizing, N, r, and k_- are kept fixed and we explore the parameter space α, β, and D within the ranges and constraints mentioned above. In every particular situation we determine the value of k_+, see Eq. (3.18), in order to keep $\langle c_A \rangle = 25$ nM.

3.2.4 Passive versus Active Transport in QS

The rate of passive diffusion has been estimated for the 3-oxo-C6-AHL autoinducer [9]: $\sim 10^3$ min^{-1}. Under these conditions the typical value for the normalized parameter $\tilde{D}$ is of the order of 10^4. Yet, active transport mechanisms for the autoinducer lead to much smaller effective diffusion values. For example, in the bacterial species *Pseudomonas aeruginosa*, C4-HSL can freely diffuse but C12-HSL, a larger signaling molecule, is subjected to active influx and efflux where its importation and exportation rates are of the order of $\sim 10^{-2}$ min^{-1} and $\sim 10^{-1}$ min^{-1}, respectively [29]. Other example corresponds to the AI-2 signaling molecule. The latter is present in many Gram-positive and Gram-negative species and it is believed to allow for interspecies communication [30]. In *Escherichia coli* and *Salmonella enterica* extracellular AI-2 accumulates during the exponential phase, but then decreases drastically upon entry into the stationary phase. This reduction is due to the import and processing of AI-2 by the Lsr transporter [30,31]. Moreover, excretion from the cell of this autoinducer also appears to be an active process involving the putative transport protein YdgG (or alternatively named TqsA) [32]. In the case of *E. coli* these rates have been estimated by computational and experimental means: $D_{\text{out}} \simeq 10^{-1}$ min^{-1} and $D_{\text{in}} \simeq 10^{-3} - 10^{-2}$ min^{-1} [33].

In principle our model does not account for active diffusion processes, but transport driven by concentration differences. Still, our simple model is valid when the active transport mechanism can be described by two symmetric first-order transport reactions. If we assume that the excretion and uptake systems follow the Michaelis–Menten kinetics then, in the regime where the concentration of autoinducer (substrate) is much smaller than the K_m of the enzymatic reaction, the transport rate can be approximated by a first-order reaction with rates $D_{\text{in}} c_{A_{\text{ext}}}$ and $D_{\text{out}} c_a$. If, in addition, we assume that the transport rates are symmetric, $D_{\text{in}} = D_{\text{out}}$, the resulting dynamics are identical to the case of passive diffusion. Under these conditions, the rates of active transport in the QS systems described above would fit in our model with a normalized diffusion coefficient in the range $\tilde{D} \in [10^{-1}, 10]$. All in all, the transport rates when driven by active processes are four orders of magnitude smaller than the diffusion rate of small molecules through the membrane. Hence, transport rates in QS systems can be categorized into two main, well-separated, classes: small transport rates due to active process, and large diffusion rates due to passive mechanisms.

3.2.5 Dynamics and Population Heterogeneity driven by Diffusion

According to the analytical results, as a function of $\tilde{D}$ one can expect a rich phenomenology since the transition lines in the parameter space $(\tilde{\alpha}, \tilde{\beta})$ shift as a function of the diffusion (see Fig. 3.2a). By taking as a reference the case

γ_2, that is $(\tilde{\alpha}, \tilde{\beta}) = (15, 5)$, Fig. 3.3 shows the effect of the diffusion on the distribution (left column) and dynamics (center column) of c_A in a given cell. The results were obtained by means of numerical simulations of the set of reactions (3.1)–(3.5) using the Gillespie algorithm in an N-cells system [34]. The system initially displays a single-peak distribution and by increasing the diffusion rate we observe transitions to other behaviors (monotonically decreasing and double-peak distributions). For $\tilde{D} = 10$, the diffusion is already large enough to remove signaling molecules between consecutive mRNA burst events, thus leading to a monotonically decreasing distribution. Increasing the diffusion rate to $\tilde{D} = 100$ leads to the situation where both $\tilde{\alpha}$ and $\tilde{\beta}$ become smaller than $1 + \tilde{D}$ and a bistable dynamics develops. Note that, counterintuitively, increasing the diffusion leads to a population heterogeneity instead of homogenizing the colony. As the diffusion further increases, e.g. $\tilde{D} = 2 \cdot 10^3$, the autoinducer molecules diffusing from the external medium into the cell set a constitutive level of this species. The latter explains the presence of A molecules in the cell even if no mRNA is produced. Finally, at very large values of $\tilde{D}$, e.g. $\tilde{D} = 5{\cdot}10^4$, the low constitutive concentration of the autoinducer increases due to the influx of molecules when no mRNA is present whereas the concentration of A that is internally produced decreases due to the efflux of molecules. In this case, the whole N-cells system can be considered as a single volume with no diffusive barriers between cells. Thus, the burst events average out and, as a consequence, a single effective peak again develops for the concentration of the autoinducer.

Figure 3.3 shows that the theoretical distribution captures the essential features of the dynamics obtained in the numerical simulations. Note that the noticeable deviations are due to the intrinsic noise (i.e., to the low number of molecules) of the signaling molecule A that are not considered in the theoretical analysis. Moreover, notice that as the diffusion increases those deviations seem to be larger. Yet, we stress that as $\tilde{D}$ changes we modulate the production rate k_+ so that the average number of autoinducer molecules per cell remains constant. Consequently, the deviations between the simulations and the theoretical analysis cannot be ascribed to a putative decrease of the number of A molecules (i.e., to an increase of the intrinsic noise).

In order to ensure that the intrinsic fluctuations are not actually increasing due to diffusion we first perform the following *in silico* control experiment. We consider a modification of the system such that a single mRNA molecule transcript leads to two autoinducer molecules that are considered to be distinguishable: A_1^i and A_2^i. Following [35], by plotting the distribution of c_{A_1} as a function of c_{A_2} we can then discern a putative increase of the intrinsic fluctuations. Right column of Fig. 3.3 shows that the width of the distribution in a direction perpendicular to the diagonal (a measure of the intrinsic fluctuations) does not vary and consequently so does not the intrinsic noise. Thus, we must conclude that as the diffusion increases the balance between the mRNA and the intrinsic fluctuations get modified. Indeed, as shown in Eq. (3.22) the noise due to the mRNA dynamics behaves as $\sim 1/\tilde{D}$ for large values of $\tilde{D}$. Therefore, the deviations between the theoretical and the numerical

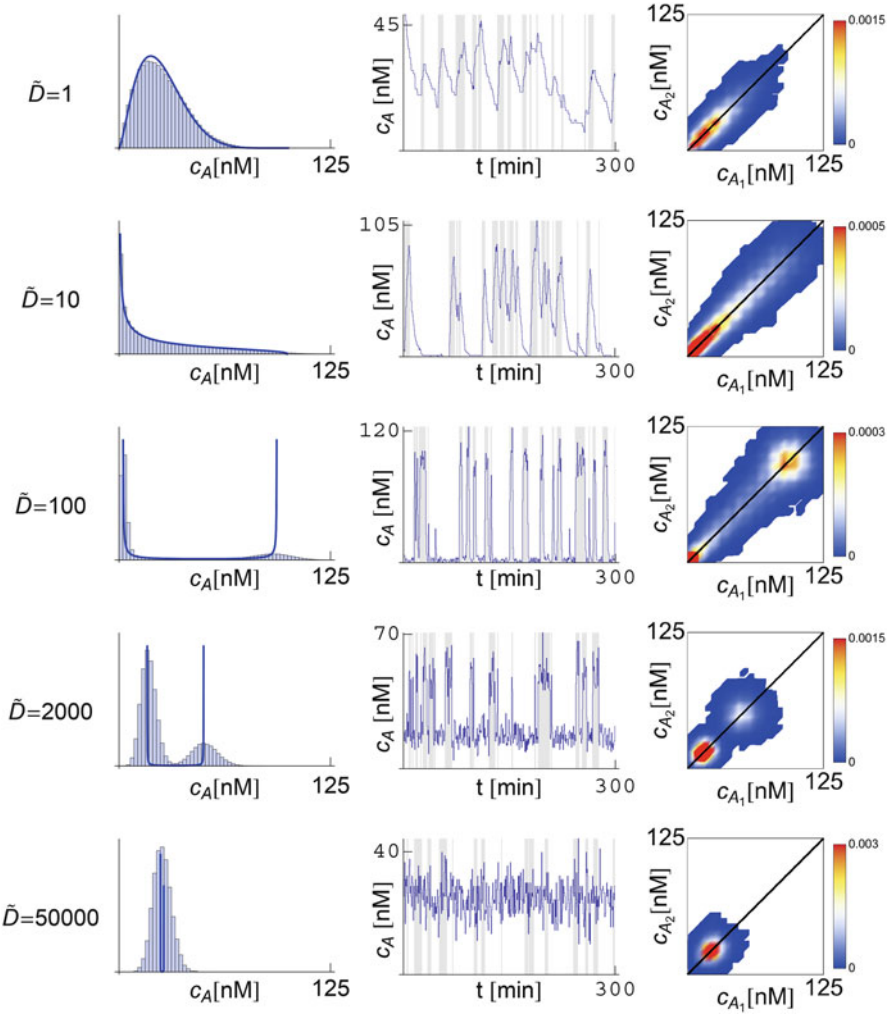

Fig. 3.3 Distributions and dynamics of the signaling molecule. Distributions (*left column*) and dynamics (*center column*) of c_A at steady-state for different values of $\tilde{D}$. In all cases the parameters set $(\tilde{\alpha}, \tilde{\beta})$ is γ_2 (see Fig. 3.2b). The production rate $\tilde{k}_+$ is modulated as a function of $(\tilde{\alpha}, \tilde{\beta}, \tilde{D})$ in order to maintain constant the average $\langle c_A \rangle = 25$ nM. The histograms obtained in the stochastic simulations (*blue bars, left column*) are in qualitative agreement with the probability densities from the analytical calculations (*blue line, left column*). When increasing the diffusion coefficient the system explores different dynamics as revealed by the trajectories shown in the center column. The *gray-shaded background* shown in the trajectories of c_A indicates the presence of an mRNA molecule in the cell. In order to discern a putative increase in the molecular noise we perform stochastic simulations of a modified system in which a single mRNA molecule produces two distinguishable autoinducer molecules A_1 and A_2. The density plots (*right column*) of the distribution of c_{A_2} vs c_{A_1} reveal that the diffusion does not contribute to an increase of the intrinsic noise since the spreading of the distributions in a direction perpendicular to the diagonal does not grow when increasing $\tilde{D}$

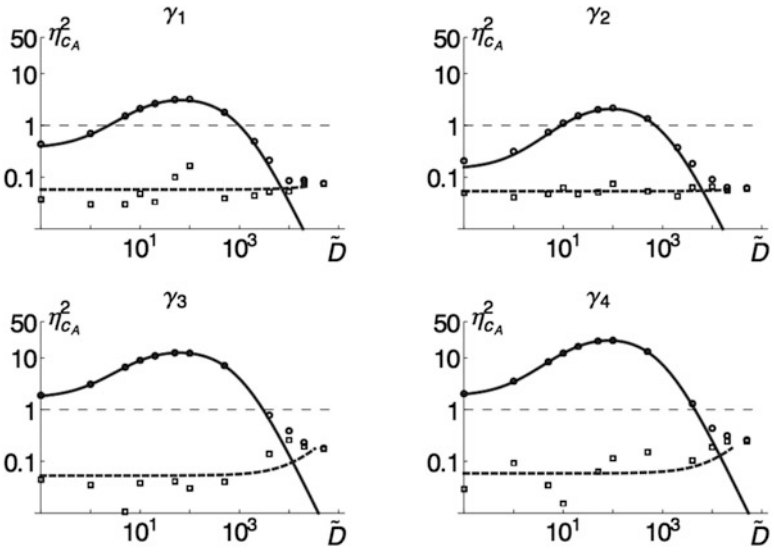

Fig. 3.4 Total noise in the signaling molecule as a function of the diffusion coefficient. Total noise $\eta^2_{c_A}$ as a function of diffusion coefficient $\tilde{D}$ for the sets of parameters $\gamma_{1,2,3,4}$ (see Fig. 3.2b): stochastic simulations (*circles*) and analytical expression (3.22) (*solid line*). The difference between the computational and the theoretical distributions quantifies the amount of intrinsic noise (*squares*). The latter remains constant and is the main contribution to the total noise only for large diffusion values, $\tilde{D} > 10^4$. The function is non-monotonic and has a maximum value above $\eta^2_{c_A} > 1$ for all parameter sets, showing that the variance is larger than the mean for intermediate ranges of $\tilde{D}$

approaches are due to a drop of the fluctuations related to the mRNA dynamics such that for large enough diffusion rates, the intrinsic noise constitutes the main source of stochasticity.

3.2.6 Total Noise in QS Communication Lacking Autoinduction

It is interesting to place these results in the context of the total noise present in the autoinducer concentration. Figure 3.4 reveals that $\eta^2_{c_A}$ shows a non-monotonic behavior. As a function of $\tilde{D}$ the total noise first increases and reaches a maximum at $\tilde{D} \sim 10^2$ and then decreases as the diffusion becomes larger. Note that for a large range of $\tilde{D}$ values the analytical calculations, that just account for the transcriptional noise, are in agreement with the numerical simulations, that account for both the transcriptional and the intrinsic noise. This indicates that the main contribution to the total fluctuations for a large range of diffusion values is the transcriptional noise. Yet, as mentioned above, the latter diminishes as the diffusion increases while the

intrinsic fluctuations remain constant. Consequently, the contribution of the intrinsic noise must become more relevant than the mRNA stochasticity beyond some value of $\tilde{D}$. One can address the relative importance of the noisy sources by using the decomposition $\eta^2_{c_A} = \eta^2_{c_A,\text{int}} + \eta^2_{c_A,\text{tran}}$, where $\eta^2_{c_A,\text{int}}$ and $\eta^2_{c_A,\text{tran}}$ stand, respectively, for the intrinsic and the transcriptional contributions to the total noise [36]. Thus, by subtracting the analytical expression of the transcription noise given by Eq. (3.22) to the total noise obtained in the numerical simulations we are able to compute the intrinsic noise as a function of the diffusion (see Fig. 3.4). By performing a linear regression of the points that corresponds to the intrinsic noise we obtain that the slope of the curve is indeed zero in practical terms ($2 \cdot 10^{-7}$ for parameter set γ_2). Therefore, in agreement with the results obtained in Fig. 3.3 (right column), the intrinsic noise remains constant ($\eta^2_{c_A,\text{int}} = 0.054 \pm 0.003$ for parameter set γ_2) as the diffusion increases and is the main stochastic component if $\tilde{D} \gtrsim 10^4$.

The non-monotonic behavior of the total noise as a function of the diffusion rate suggests a new interpretation of the role of noise regulation by the QS mechanism. As mentioned above, the values of the diffusion rates in QS systems fall into two distinctive categories: either large values corresponding to passive transport mechanism, $\tilde{D} \sim 10^4$, or small values when an active transport mechanism applies, $\tilde{D} \sim 10^{-1} - 10$. Surprisingly, these two QS classes avoid diffusion rates that maximize the total noise, $\tilde{D} \sim 5 \cdot 10^1 - 10^2$. While the modeling presented herein is certainly very simple and the derived consequences should be carefully taken, the latter suggests that bacteria have developed mechanisms for coping with the noise and keep their functional QS regime away from the region where $\eta^2_{c_A} > 1$. Notice that the maximum noise in the level of autoinducer means large fluctuations that may perturb the activation of the QS pathway. When looking at the dynamics of the autoinducer for $\tilde{D} = 100$ (see Fig. 3.3) we observe the population heterogeneity such that the autoinducer "jumps" between a low state with few molecules and a high state around 100 nM. If the activation threshold lies in between these two values (as it actually does), the QS pathway could get randomly activated due to the fluctuations only in a subpopulation and the colony would lack a synchronous behavior. Yet, our results point towards the direction that bacteria have adapted their communication mechanisms in order to improve the signal-to-noise ratio and produce a more reliable information exchange.

In the next section we further explore the relation between noise, network architecture, and synchronous collective behavior by introducing the concept of precision in a more detailed model.

3.3 Non-stationary Signaling, Network Structure, and Noise

The seminal work of Nealson and coworkers described the QS phenomenon as a *sudden* activation of the bioluminescence in a culture of growing *V. fischeri* cells [37]. It was not until recently that the behavior of individual cells has been shown

to differ significantly from the bulk behavior, revealing large inter-cell variations in the expression level of QS genes. Thus, Pérez and Hagen [38] were able to measure the weak bioluminescence of a single bacterium and observed a large cell-to-cell variability in the level of emission and in the onset time for the response. Importantly, this heterogeneity seemed not to be related to the specificities of *V. fischeri* and has been also reported in other QS bacterial species, as *Vibrio harveyi* [39], *P. aeruginosa* [40], and synthetic *E. coli luxI/luxR-GFP* strains [41].

As shown above, noise plays an important role in the QS activation phenomenon and the aforementioned cell-to-cell heterogeneity may be caused by the random fluctuations that unavoidably affect cell regulation and signaling. Yet, answering this question in deep requires a case-dependent approach since the underlying network architecture conditions how noise is filtered, enhanced, and/or suppressed. Moreover, many QS systems may sense and use different autoinducers and the design principles of these multi-input systems remain puzzling particularly in the framework of QS stochasticity. Recent advances include the study of *V. fischeri* cells that is regulated by two HSL signals. The results show that at the single-cell level the heterogeneity in the lux response depends only on the average degree of activation, so that the noise in the output is not reduced by the presence of the second signal [42]. Still, most QS systems share the same underlying network motif, a two component positive feedback loop. Thus, by studying a canonical QS system one can address questions and raise conclusions about the relation between network architecture and noise regulation.

In *V. fischeri* cells, the canonical activation pathway is controlled by LuxR, the receptor of the signaling molecule, and LuxI, the synthetase of the signaling molecules. Therefore, fluctuations at the expression levels of these two proteins can potentially influence the variability in the QS transition. Interestingly, experiments have revealed the presence of additional regulatory interactions for controlling the LuxR noise levels [44]. Yet, the regulatory interactions that control the wild-type lux operon in *V. fischeri* are more complex than first thought [45,46]. Those include both positive and negative regulation of the *luxR* gene depending on the concentration of the autoinducer [47]. In this regard, simplified synthetic constructs in *E. Coli*, such as *lux01* and *lux02* [43], retain the minimal LuxI/LuxR regulatory motif and lack the structural genes responsible for light emission that may also play a regulatory role, e.g. *luxD* [48]. These constructs reproduce the main features of the wild-type operon as revealed by the GFP fluorescence assays reporting the promoter activity [43]. In this section, we make use of the simplified network architecture of these synthetic strains in order to study how the cell-to-cell variability changes when we modulate independently the intensity of gene expression noise of LuxR and LuxI and raise general conclusions about the relation between noise and network architecture.

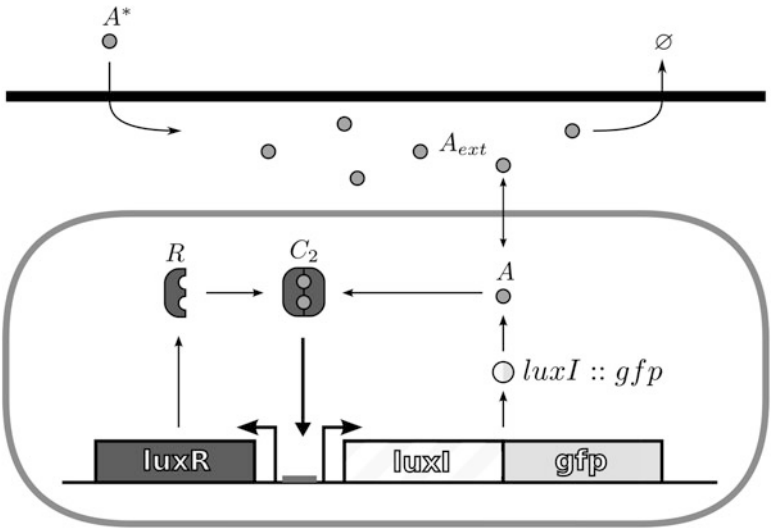

Fig. 3.5 Scheme of the LuxI/LuxR regulatory network in lux01 and lux02 strains. The LuxR (R) protein activates the operon upon binding to autoinducer molecules (A). The *lux01* operon lacks the *luxI* gene and therefore cells cannot produce their own autoinducer and exogenous signaling molecules, A^*, are needed to activate the expression of *luxR* and GFP [43]. On the other hand, the *lux02* operon carries a *luxI::gfp* fusion and allows for the production of autoinducer and self-induction

3.3.1 Synthetic Strains: A LuxR/LuxI System with No Frills

The *lux01* operon is a truncated divergently transcribed *lux* operon, capable of expressing LuxR but lacking the *luxI* gene. All the transcripts normally downstream of the promoter are replaced with *gfp*. Thus, bacteria carrying the *lux01* operon cannot produce the autoinducer and an exogenous autoinducer is required for GFP expression. On the other hand, the *lux02* operon carries a *luxI::gfp* fusion and is capable of expressing LuxI and synthesize the autoinducer [43]. Figure 3.5 shows schematically the regulatory interactions present in these strains as well as the control of the autoinducer levels by means of exogenous signaling molecules. These interactions and the *DNA* duplication process can be formally written as a set of chemical reactions:

$$
\begin{aligned}
DNA &\xrightarrow{\alpha_R k_R} DNA + mRNA_{\text{luxR}} \\
DNA &\xrightarrow{\alpha_I k_I} DNA + mRNA_{\text{luxI::gfp}} \\
DNA \cdot (luxR \cdot A)_2 &\xrightarrow{k_R} DNA \cdot (luxR \cdot A)_2 + mRNA_{\text{luxR}} \\
DNA \cdot (luxR \cdot A)_2 &\xrightarrow{k_I} DNA \cdot (luxR \cdot A)_2 + mRNA_{\text{luxI::gfp}}
\end{aligned}
$$

$$
\begin{aligned}
mRNA_{\text{luxR}} &\xrightarrow{p_R} mRNA_{\text{luxR}} + luxR \\
mRNA_{\text{luxI::gfp}} &\xrightarrow{p_I} mRNA_{\text{luxI::gfp}} + luxI::gfp \\
luxI::gfp &\xrightarrow{k_A} A + luxI::gfp \\
luxR + A &\underset{k_1^-}{\overset{k_1^-/K_{d1}}{\longleftrightarrow}} luxR \cdot A \\
2\,(luxR \cdot A) &\underset{k_2^-}{\overset{k_2^-/K_{d2}}{\longleftrightarrow}} (luxR \cdot A)_2 \\
(luxR \cdot A)_2 + DNA &\underset{k_{\text{lux}}^-}{\overset{k_{\text{lux}}^-/K_{\text{dlux}}}{\longleftrightarrow}} DNA \cdot (luxR \cdot A)_2 \\
A &\underset{rD}{\overset{D}{\longleftrightarrow}} A_{\text{ext}} \\
A &\xrightarrow{d_A} \varnothing \\
A_{\text{ext}} &\xrightarrow{d_A} \varnothing \\
mRNA_{\text{luxR}} &\xrightarrow{d_{\text{mR}}} \varnothing \\
mRNA_{\text{luxI::gfp}} &\xrightarrow{d_{\text{mI}}} \varnothing \\
luxR &\xrightarrow{d_R} \varnothing \\
luxI::gfp &\xrightarrow{d_I} \varnothing \\
(luxR \cdot A)_2 &\xrightarrow{d_{C_2}} \varnothing \\
luxR \cdot A &\xrightarrow{d_C} \varnothing \\
DNA &\xrightarrow{ln(2)/\tau} DNA + DNA \\
DNA \cdot (luxR \cdot A)_2 &\xrightarrow{ln(2)/\tau} DNA \cdot (luxR \cdot A)_2 + DNA.
\end{aligned}
\tag{3.23}
$$

As revealed by the set of reactions (3.23) the regulatory complex $(luxR \cdot A)_2$ activates the transcription of both *luxI* and *luxR* upon binding to the *DNA*. Since *lux01* lacks the *luxI* gene, the autoinducer, A, cannot be synthesized, i.e. in that case $k_A = 0$. Note that in agreement with Sect. 3.2.1, we include basal transcriptional rates, $\alpha_R k_R$ and $\alpha_I k_I$, even though the regulatory complex $(luxR \cdot A)_2$ is not bound to the promoter region of the *DNA*.

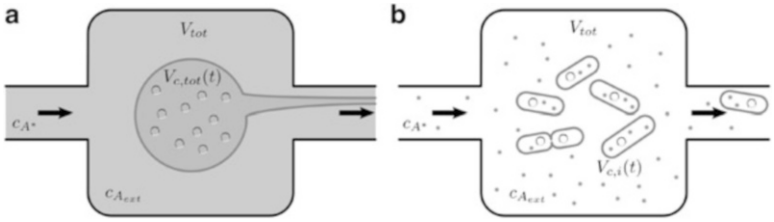

Fig. 3.6 Scheme of the deterministic and stochastic modeling approaches. (**a**) In the deterministic model, the population of cells is described by a unique volume with average and continuous concentrations of all species, including the DNA carrying the QS network (*small circles*). Cellular growth is also taken into account in this approach. (**b**) In the stochastic model, cells are modeled as individual compartments that can grow and divide and all molecular species are represented as discrete entities. In both cases we assume that all species are well stirred inside the cells and in the medium. In order to maintain a constant cell density, as in the experiments we aim to model, a dilution protocol is implemented (see text). In the deterministic model the dilution removes continuously cytoplasmic material in order to compensate the cell growth. In the stochastic model individual cells are removed every time a new cell is born

3.3.2 *Bulk and Single-Cell Approaches: Cell Growth, Division, and External Dilution Protocol*

The set reactions (3.23) can be sampled exactly by means of the Gillespie algorithm [34] (stochastic approach). The latter is suitable for the characterization of the system at the single cell level. Complementary to this, if we consider the colony as a whole and the number of molecules of the species is large enough, we can assume that intrinsic fluctuations average out and the set of ordinary differential equations (ODEs) that derive from reactions (3.23) describe the bulk behavior (deterministic description). Still, as shown below in Sect. 3.3.6, the intrinsic fluctuations can actually modify the behavior of the system in a more profound way. Herein we make use of both deterministic and stochastic descriptions. The former is particularly useful to fit the simulation results to experimental data in order to obtain values of the parameters.

As for the deterministic model, we consider that all cells share their cytoplasm in a *single* volume $V_{c,\mathrm{tot}}$ (see Fig. 3.6). Chemical species X inside *the* cell are described by their concentration, c_X, in $V_{c,\mathrm{tot}}$ and the chemical kinetics formalism leads to a set of ODEs that describes the population average dynamics:

$$\dot{c}_{\mathrm{luxI::gfp}} = p_I c_{mRNA_{\mathrm{luxI::gfp}}} - \left(\frac{ln(2)}{\tau} + d_I\right) c_{\mathrm{luxI::gfp}} \tag{3.24}$$

$$\dot{c}_{\mathrm{luxR}} = -\frac{k_1^-}{K_{d1}} c_A c_{\mathrm{luxR}} + k_1^- c_{\mathrm{luxR}\cdot A} + p_R c_{\mathrm{mRNA_{luxR}}} - \left(\frac{ln(2)}{\tau} + d_R\right) c_{\mathrm{luxR}} \tag{3.25}$$

$$\dot{c}_{\mathrm{mRNA_{luxI::gfp}}} = \alpha_I k_I c_{\mathrm{DNA}} + k_I c_{\mathrm{DNA}\cdot(\mathrm{luxR}\cdot A)_2} - \left(\frac{ln(2)}{\tau} + d_{\mathrm{mI}}\right) c_{\mathrm{mRNA_{luxI::gfp}}} \tag{3.26}$$

$$\dot{c}_{\text{mRNA}_{\text{luxR}}} = \alpha_R k_R c_{\text{DNA}} + k_R c_{\text{DNA}\cdot(\text{luxR}\cdot A)_2} - \left(\frac{ln(2)}{\tau} + d_{\text{mR}}\right) c_{\text{mRNA}_{\text{luxR}}} \tag{3.27}$$

$$\dot{c}_{\text{luxR}\cdot A} = -k_1^- c_{\text{luxR}\cdot A} + \frac{k_1^-}{K_{d1}} c_A c_{\text{luxR}} - 2\frac{k_2^-}{K_{d2}} [c_{\text{luxR}\cdot A}]^2 + 2k_2^- c_{(\text{luxR}\cdot A)_2} \tag{3.28}$$

$$- \left(\frac{ln(2)}{\tau} + d_C\right) c_{\text{luxR}\cdot A} \tag{3.29}$$

$$\dot{c}_{(\text{luxR}\cdot A)_2} = \frac{k_2^-}{K_{d2}} [c_{\text{luxR}\cdot A}]^2 - k_2^- c_{(\text{luxR}\cdot A)_2} - \frac{k_{\text{lux}}^-}{K_{\text{dlux}}} c_{(\text{luxR}\cdot A)_2} c_{\text{DNA}} \tag{3.30}$$

$$+k_{\text{lux}}^- c_{\text{DNA}\cdot(\text{luxR}\cdot A)_2} - \left(\frac{ln(2)}{\tau} + d_{C_2}\right) c_{(\text{luxR}\cdot A)_2} \tag{3.31}$$

$$\dot{c}_{\text{DNA}} = -\frac{k_{\text{lux}}^-}{K_{\text{dlux}}} c_{(\text{luxR}\cdot A)_2} c_{\text{DNA}} + k_{\text{lux}}^- c_{\text{DNA}\cdot(\text{luxR}\cdot A)_2} \tag{3.32}$$

$$+\frac{ln(2)}{\tau} \left(c_{\text{DNA}} + c_{\text{DNA}\cdot(\text{luxR}\cdot A)_2}\right) - \frac{ln(2)}{\tau} c_{\text{DNA}} \tag{3.33}$$

$$\dot{c}_{\text{DNA}\cdot(\text{luxR}\cdot A)_2} = \frac{k_{\text{lux}}^-}{K_{\text{dlux}}} c_{(\text{luxR}\cdot A)_2} c_{\text{DNA}} - k_{\text{lux}}^- c_{\text{DNA}\cdot(\text{luxR}\cdot A)_2} - \frac{ln(2)}{\tau} c_{\text{DNA}\cdot(\text{luxR}\cdot A)_2} \tag{3.34}$$

$$\dot{c}_A = k_1^- c_{\text{luxR}\cdot A} - \frac{k_1^-}{K_{d1}} c_A c_{\text{luxR}} + k_A c_{\text{luxI::gfp}} + D\left(c_{A_{\text{ext}}} - c_A\right) \tag{3.35}$$

$$- \left(\frac{ln(2)}{\tau} + d_A\right) c_A \tag{3.36}$$

$$\dot{c}_{A_{\text{ext}}} = rD\left(c_A - c_{A_{\text{ext}}}\right) + \gamma \frac{V_{\text{tot}}}{V_{\text{ext}}} c_{A^*} - (\gamma + d_A) c_{A_{\text{ext}}} \tag{3.37}$$

The experiments reveal that the temporal scale for reaching a steady-state is much larger than the cell cycle duration (see, for instance, Figure S6 in [43]). Thus, we need to take into account the cell growth. If cells are maintained in the exponential phase with doubling time τ, then the dynamics of the volume of *the* cell is $V_{c,\text{tot}}(t) = V_{0,\text{tot}} 2^{t/\tau}$, where $V_{0,\text{tot}} = N V_0$, N being the number of cells in the colony and V_0 the volume of a single cell at the beginning of the cell cycle. As a consequence, the cellular growth introduces dilution terms, $-c_X \frac{ln(2)}{\tau}$, in the r.h.s. of the ODEs of all species, with the exception of the autoinducer in the medium A_{ext}. On the other hand, cell division events lead to the duplication of the genetic material. The latter is taken into account by adding the term $+\frac{ln(2)}{\tau}\left(c_{\text{DNA}} + c_{\text{DNA}\cdot(\text{luxR}\cdot A)_2}\right)$ to the ODE that describes the concentration of *DNA*. Note that this term compensates for the dilution.

In the experiments that reported the properties of the *lux01* and *lux02* QS strains the cell density is kept constant by means of an external dilution protocol that compensates for cell proliferation [43]. In order to compare quantitatively with those experiments, we keep the volume $V_{c,\text{tot}}$ constant and define the external volume, V_{ext}, such that the total volume of the cell culture reads $V_{\text{tot}} = V_{\text{ext}} + V_{c,\text{tot}}$. Accordingly, the parameter r, see reactions (3.23), reads $r = V_{c,\text{tot}}/V_{\text{ext}}$. Notice that the external dilution protocol also removes from the medium autoinducer molecules [43]. This is

compensated by an influx of exogenous autoinducer in the dilution buffer. The influx of exogenous autoinducer molecules, together with the efflux of culture medium, can be represented by the following reaction

$$A_{\text{ext}} \underset{\gamma c_{A^*} V_{\text{tot}}}{\overset{\gamma}{\longleftrightarrow}} \varnothing. \tag{3.38}$$

where $\gamma = ln(2)/\tau$. That is, an efflux removes autoinducer molecules from the external volume at a rate γ and an influx introduces signaling molecules in the external volume at a rate $\gamma c_{A^*} V_{\text{tot}}$. In the deterministic description, this reaction leads to an additional term at the r.h.s. of the ODE for the concentration of A_{ext} : $+\gamma \left(c_{A^*} \frac{V_{\text{tot}}}{V_{\text{ext}}} - c_{A_{\text{ext}}} \right)$. In the absence of synthesis (e.g., *lux01* strain) and taking into account that the degradation is slower than the diffusion and the influx rate, it is easy to see that the concentration of autoinducer, both inside and outside *the* cell, tends to c_{A^*}: the desired control value of the autoinducer concentration.

As for the single-cell, stochastic, description, each bacterium is described as a single cell carrying a copy of the regulatory network. As in the deterministic case, cell growth introduces a dilution of the molecules in a cell. Cell growth is implemented by allowing the volume of cell i to change in time as

$$V_{c,i}(t) = V_0 2^{t/\tau_i}, \tag{3.39}$$

where V_0 is the volume of a cell at the beginning of the cell cycle, τ_i is the duration of the cell cycle of cell i, and t is referred to the precedent division event. When $t = \tau_i$ the cell i has doubled its volume and a new division takes place. At this time the internal clocks and volumes of daughter cells are reset to zero and V_0, respectively. The duration of the cell cycle, τ_i, is different for each cell and is set independently after a division according to the following stochastic rule [49],

$$\tau_i = \lambda \tau + (1 - \lambda) \tilde{\tau}, \tag{3.40}$$

where τ and $\tilde{\tau}$ denote, respectively, the deterministic and stochastic components of the cell cycle duration, and $\lambda \in [0, 1]$ is a parameter that weights their relative importance. The stochastic component accounts for the period of time between events driven by a Poissonian process and satisfies an exponential distribution,

$$\rho(\tilde{\tau}) = \frac{e^{-\frac{\tilde{\tau}}{\tau}}}{\tau}. \tag{3.41}$$

According to these definitions, the average duration and standard deviation of the cell cycle are τ and $(1 - \lambda)\tau$, respectively. When a cell divides, proteins, mRNAs, and signaling molecules inside the cell are binomially distributed [50] between daughter cells and one copy of the DNA is given to each cell (regulatory complexes bound to the DNA are detached prior to the distribution between daughter cells).

As in the case of the deterministic description, the cell density is kept constant due to a compensating efflux that wash away cells in the culture: each time a division takes place a cell is picked at random and "deleted." In relation to the effect of the cell volume of individual cells on the diffusion rate of the autoinducer, we note that in this case

$$r_i(t) = \frac{V_{c,i}(t)}{V_{\text{tot}} - \sum_{j=1}^{N} V_{c,j}(t)}. \tag{3.42}$$

A model as comprehensive as the one introduced here requires to know the value of a large number of parameters. Some of those have been characterized and measured in previous experiments, e.g. the dissociation constant of LuxR to A [51], while others have to be estimated or fitted. In the case of the synthetic strains reviewed herein most of the parameters can be estimated by fitting the results obtained in numerical simulations of the deterministic system to experimental data reporting on the colony bulk behavior [43]. We refer the reader to [18] for the fitting procedure and the list of estimated parameters.

3.3.3 Noise Intensity Regulation: Burst Size

In experiments there are two possible ways to regulate the intensity of the intrinsic noise keeping the same average values of protein concentration. On the one hand, one can scale up the number of molecules and the volume while keeping the same ratio, i.e. the same concentration. This approach has been indeed implemented in bacterial cultures by inhibiting the septation process [52]. The downside of this method is than one cannot actually control the noise level since during the time course of an experiment it diminishes progressively. On the other hand, one can control the so-called burst size that quantifies the translational efficiency. During translation mRNA molecules are translated into proteins following a bursting dynamics [3, 20, 53]. The so-called burst size, b_X, is defined as the ratio between the protein X production rate and the mRNA X degradation rate. It has been shown that b_X is directly related to the intensity of gene expression noise [54]. Thus, for the same average protein concentration, the larger b_X, the more fluctuating is the expression dynamics of X. Herein we use this approach and tune independently the noise intensity of *luxI* and *luxR* in our simulations in order to elucidate the role of fluctuations at the level of the main components of the QS switch architecture. Unless explicitly indicated otherwise, the bursting size in the stochastic simulations is $b_R = b_I = 20$ [44, 53].

3.3.4 LuxR Noise Levels and the Induction Time Control the Features of the QS Switch

In order to analyze the behavior of individual cells and reveal how noise affects the QS switch, we perform stochastic simulations of a population of growing and dividing cells. As described above, the *in silico* cell culture grows in a medium at a (nearly) fixed autoinducer concentration. We measure the activation of the QS network by reporting the concentration of GFP in single cells. The transition of an individual cell between the low (no signal from the GFP reporter) and the high state (signal from the GFP reporter) is intrinsically random and depends, among others, on the levels of autoinducer. Thus, inside a population some cells will jump while others remain in their current state leading to a bimodal phenotypic distribution. We compute the proportion of cells that are below and above a threshold of GFP equal to half-maximum GFP concentration; we consider the distribution of cells to be bimodal when the proportion of cells in either the low or the high state is below 90 %. According to this, we define the range of autoinducer concentration $[c_{A^*_{b1}}, c_{A^*_{b2}}]$ for which there is bimodality. For low concentrations of autoinducer, $c_{A^*} < c_{A^*_{b1}}$, the collective response of the cell population is unactivated, and for high concentrations, $c_{A^*} > c_{A^*_{b2}}$, most of the cells are activated leading to a global response of the colony. On the other hand, within the bimodality range, the response is distributed between two subpopulations, thus failing to achieve a global coordination in the colony. In order to characterize this behavior, we introduce the concept of *precision* in the QS switch as the inverse of the c_{A_*} concentration range for which the cells response distribution (phenotypes) is bimodal. That is, the larger the bimodal range, the less precise the switch is in order to generate a global response in the colony. We point out that the precision of the switch in a noise-free situation (deterministic case) is infinite since all cells achieve global coordination simultaneously.

Figure 3.7 shows, by means of a color density plot, the probability of a cell to have a particular GFP expression level after either 10 or 100 h of induction as a function of c_{A^*}. For a large range of autoinducer concentrations, both *lux01* and *lux02*, display a bimodal distribution after 10 h of induction. Some cells of the colony are induced at a concentration lower than the critical concentration of the deterministic model at the steady state (black line). Still, the concentration for which more than 90 % of the cells are induced requires up to four times more autoinducer than under deterministic conditions. Thus, on the one hand, noise helps cells to get induced at lower autoinducer concentrations but, on the other hand, amplifies the non-stationary effects for achieving global coordination. If the same experiment is performed with a larger induction time (100 h), the situation changes dramatically. In that case, the precision of the switch increases (tenfold change) and cells achieve global coordination at (*lux01*) or before (*lux02*) the critical deterministic concentration. In any case, the simulations reveal that the behavior of the QS switch is highly dynamic and the precision of the switch is a transient quantity that crucially depends on the duration of induction.

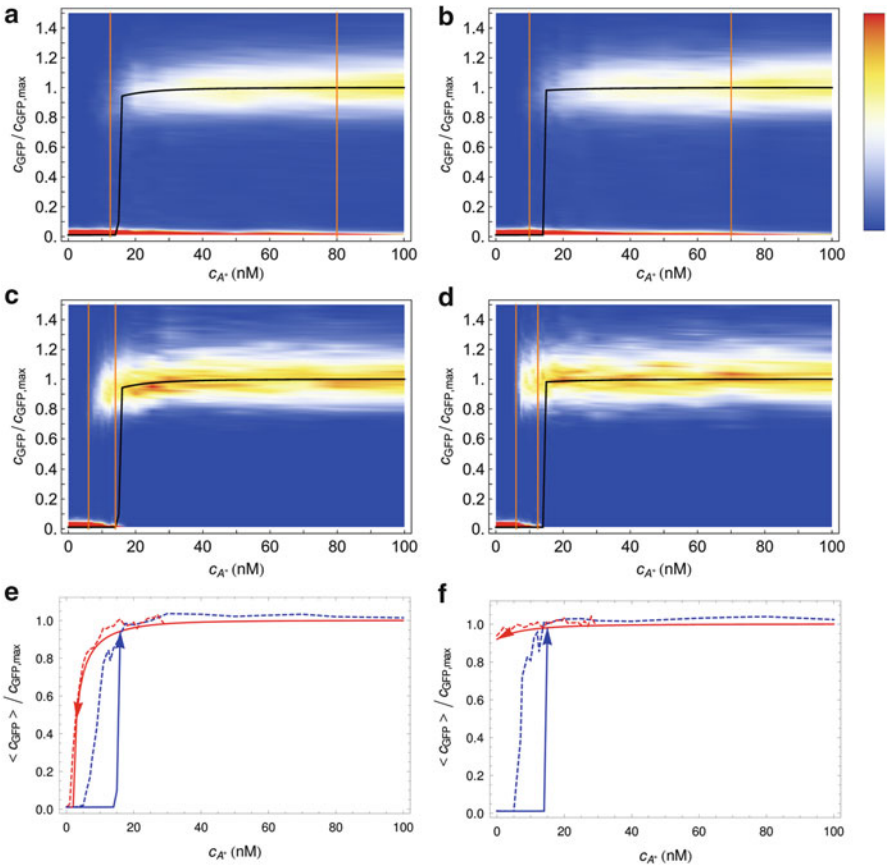

Fig. 3.7 Cell response distribution. Cell response probability after 10 h (*top*: **a**, **b**) and 100 h (*middle*: **c**, **d**) of induction at different autoinducer concentrations for the *lux01* (*left*: **a**, **c**) and *lux02* (*right*: **b**, **d**) operons in the stochastic model. The distribution reveals the coexistence of two subpopulations with low and high GFP expression when the cells are induced at intermediate autoinducer concentrations. The region of bistability (precision) is defined by the range of c_{A^*} for which the response is bimodal according to the following criterion: the lower/upper limit of the bistable region (*orange lines*) is defined by the value of c_{A^*} for which 90 % of the cells are in the low/high state. The *black line* stands for the concentration of GFP (normalized) as a function of c_{A^*} in the deterministic model at the steady state. After 10 h of induction (*top*: **a**, **b**) most cells are still in a transient state if $c_{A^*} < 70$ nM. After 100 h of induction (*middle*: **c**, **d**), the bimodality region shrinks and the precision increases. The population average curves of the induction and dilution experiments in the stochastic model (*bottom*: **e**, **f**, *dashed lines*) show that the intrinsic noise allows cells to jump to the high state inside the deterministic bistable region. On the other hand, the transition from high to low follows the deterministic path, thus indicating that the switching rate in this case is close to zero

For the same concentration of the external autoinducer, the stochastic dynamics of the regulatory network arises from the noise at the level of LuxI and LuxR. By taking the *lux02* operon as a reference case, we analyze the individual contribution

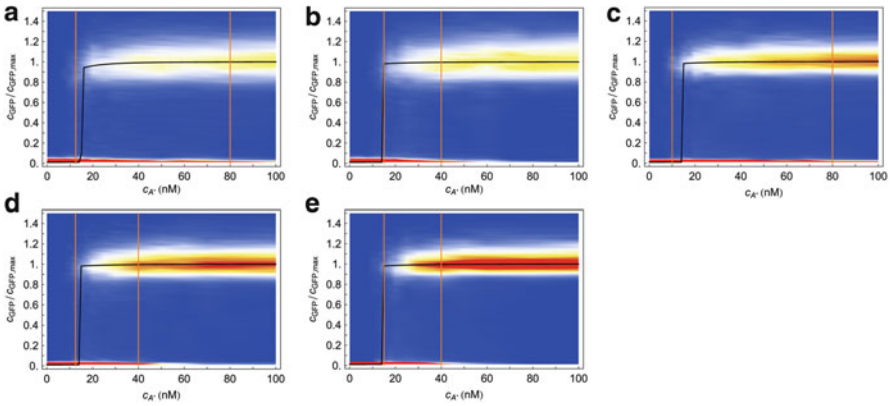

Fig. 3.8 Cell response distribution in the transient regime for different burst size values. Cell response distribution (jumping probability) after 10 h of induction (transient state) at different autoinducer concentrations for the *lux02* operon in the stochastic model and different burst sizes. Burst size values (**a**) $b_R = b_I = 20$ (**b**) $b_R = 4,\ b_I = 20$ (**c**) $b_R = 20,\ b_I = 4$ (**d**) $b_R = b_I = 4$ (**e**) $b_R = b_I = 0.01$. Width of bistable region: (**a**) = 60 nM (**b**) 25 nM (**c**) 70 nM (**d**) 27.5 nM (**e**) 25 nM. The *black line* stands for the concentration of GFP (normalized) as a function of c_{A^*} in the deterministic model at the steady state

of those network components by modulating the burst size of LuxR and LuxI (b_R and b_I, respectively). Thus, in Fig. 3.8 we plot the GFP expression probability for the *lux02* operon after 10 h of induction and for different values of the burst size b_R and b_I. Notice that the region of bimodality does not vary when changing the burst size for LuxI. However, decreasing the burst size in LuxR reduces the region of bimodality, thus increasing the precision of the switch. Furthermore, the noise at the level of LuxR helps some cells to become activated at lower concentration levels of the autoinducer. Once more, this phenomenon does not depend on the levels of noise of LuxI. That is, while the global coordination increases as the noise of LuxR decreases, more concentration of the autoinducer is required to start activating cells. On the other hand, Fig. 3.9 shows that under long induction time conditions (100 h) the precision of the switch remains constant regardless of the value of the burst size of LuxR or LuxI.

3.3.5 Activation Time Statistics: QS Cells Jump on the Bandwagon

Further insight about the role of noise of individual components and the induction time in the activation process for regulating the precision of the QS switch can be obtained by computing the so-called mean first passage time (MFPT). This quantity evaluates the average time it takes to a cell to become activated (high state)

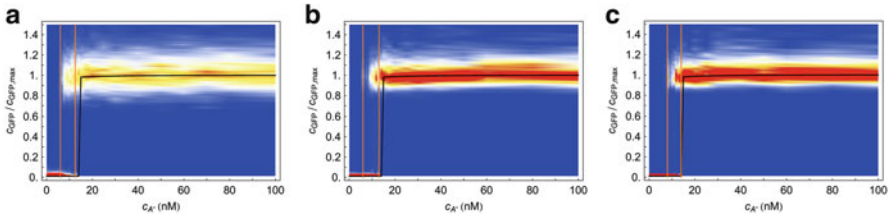

Fig. 3.9 Cell response distribution at the steady-state for different burst size values. Cell response distribution at the steady-state (100 h induction), at different autoinducer concentrations for the *lux02* operon in the stochastic model for different burst size values: (**a**) $b_R = b_I = 20$ (**b**) $b_R = b_I = 4$ (**c**) $b_R = b_I = 0.01$. The probability density of getting a particular GFP expression level is indicated by means of a density plot. The width of bistable region barely depends on the stochasticity levels, ≈ 7 nM. The *black line* stands for the concentration of GFP (normalized) as a function of c_{A^*} in the deterministic model at the steady state

starting in an unactivated situation (low state) [55]. Taking again the *lux02* case as a reference, Fig. 3.10 shows the MFPT as a function of c_{A^*} and for different values of the burst size of LuxR and LuxI. For the sake of comparison, we also compute the MFPT for the deterministic solution. As for the latter, we note that the MFPT inside the bistable region is infinite, since the deterministic system cannot spontaneously jump from one stable state to the other without the help of noise. In agreement with the results shown above, changing the burst size of LuxI does not modify the mean first passage time whereas changing the noise at the level of LuxR clearly modifies the jumping statistics. Moreover, the results reveal a nontrivial behavior of the MFPT as a function of the concentration of the autoinducer. On the one hand, with respect to the activation dynamics, when c_{A^*} is below $\sim$ 25 nM, an increase in LuxR noise decreases the mean time of the activation. That is, LuxR noise helps cells to get activated quicker. On the other hand, above $\sim$ 25 nM of autoinducer concentration, the effect is the opposite: an increase in LuxR noise slows down the cell activation. We also note that, surprisingly, when the autoinducer concentration is above the critical concentration of the deterministic system, $c_{A^*} \approx 25$ nM, the stochastic system always takes more time to get activated than the deterministic case. That is, in that case the noise does not help cells to get activated but to remain in the unactivated state.

By computing additional statistical properties of the first passage time we can clarify the behavior of the precision depending on the induction time. In particular, one can compute the times t_{low} and t_{high} for which, at a given c_{A^*} concentration, the probabilities of finding an FPT$< t_{\text{low}}$ and an FPT$> t_{\text{high}}$ are 10 %, i.e. the 10 % and 90 % quantiles, respectively. The shadings in Fig. 3.10 delimit these regions for the cases $b_R = b_I = 20$ and $b_R = b_I = 0.01$. Thus, the precision of the switch after n hours of induction is directly related to the width of the shaded region at $\langle \text{FPT} \rangle = n$ hours: at any given time, this width indicates which is the minimal concentration of autoinducer for getting 10 % of cells already activated and also the concentration beyond which more than 90 % of cells have been activated. Thus, in agreement

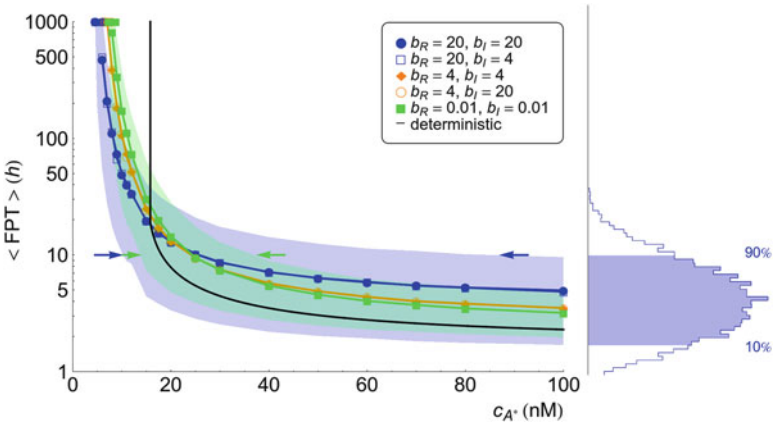

Fig. 3.10 Mean first passage time of cell activation for different burst size values for the lux02 case. Mean first passage time of cell activation (*lines*) as a function of autoinducer concentration for different values of the burst size for LuxR (b_R) and LuxI (b_I) and for the deterministic solution. The *lower* (*upper*) limit of the *shaded regions* is the 10 % (90 %) quantile curve of the distribution of FPT for the cases $b_R = b_I = 20$ (*blue shaded region*) and $b_R = b_I = 0.01$ (*green shaded region*). The distribution of the FPT for $c_{A^*} = 100$ nM, $b_R = b_I = 20$ is plotted on the side as an example. The MFPT reveals a nontrivial behavior: for low autoinducer concentration noise helps cells to jump quicker to the high state, while for high autoinducer concentration noise slows down the cells activation. Intersections of the quantile 10 % and quantile 90 % curves with a horizontal line at $t = 10$ h indicate the autoinducer concentration for which 10 % of cell trajectories have jumped to the high state (*left arrow*) and the concentration for which 90 % of cell trajectories have been activated (*right arrow*). The precision after 10 h of induction (inversely proportional to the width of the region delimited by the *arrows*) increases when decreasing the noise in LuxR

with Fig. 3.7, the induction time clearly modifies the precision: it increases (the width of the shading decreases) as the induction time becomes larger and becomes independent of the noise intensity for large induction times. Note also that as the LuxR noise weakens the precision increases.

3.3.6 *Solving a Noisy Mystery: The Fluctuations Modify the Phenotypic Landscape*

The analysis of the FPT statistics poses an intriguing question about the role of noise in the QS switch. Namely, below a "critical" concentration of autoinducer LuxR noise helps cells to become activated and above LuxR noise helps cells to remain in the unactivated state. The complexity of the detailed model presented above makes very difficult to find the reasons for this counterintuitive behavior. However, the fact that this effect is independent of the LuxI noise levels points towards the direction that the underlying reason does not depend on the communication process but on

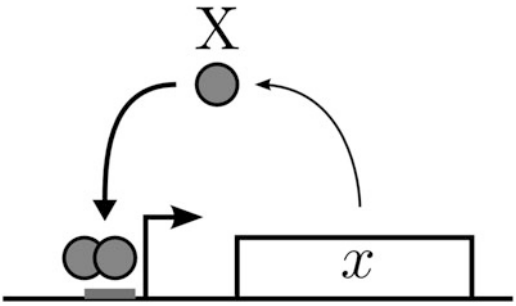

Fig. 3.11 Scheme of the genetic auto-activating switch model. The expression of gene x leads to protein X that after oligomerization binds to its own promoter acting as an self-activator

the network architecture. Therefore, we can analyze a "simple" system that shares the network motif driven by LuxR and try to draw conclusions.

The basic motif underlying regulation in QS is a positive feedback loop. In that regard, the simplest system that shares such network scheme is the so-called auto-activating switch [56, 57]. In this genetic circuit, a protein forms an oligomer that binds to the promoter region of its own gene and activates its expression (see Fig. 3.11). As shown elsewhere [16], this regulatory process can be effectively described by the Hill function formalism and leads to the following deterministic equation for the concentration, x, of protein:

$$\dot{x} = r + \frac{ax^n}{K_d + x^n} - k_5 x \tag{3.43}$$

where r is the basal expression rate (due to promoter leakiness), a the maximum production rate (efficiency of the auto-activation), n the cooperativity (oligomerization index), K_d the concentration of protein yielding half-maximum activation, and k_5 the degradation rate. In this simple model x and a play the role of the GFP expression levels and the external concentration of autoinducer in the QS switch, respectively.

Alternatively, the dimensionless version of (3.43) reads

$$\dot{\tilde{x}} = \tilde{r} + \tilde{a}\frac{\tilde{x}^n}{1 + \tilde{x}^n} - \tilde{x} \tag{3.44}$$

with $\tilde{x} = \frac{x}{\sqrt[n]{K_d}}$, $\tilde{t} = k_5 t$, $\tilde{a} = \frac{a}{k_5 \sqrt[n]{K_d}}$, $\tilde{r} = \frac{r}{k_5 \sqrt[n]{K_d}}$.

If $n \geqslant 2$ and $\left(3\sqrt{3}\right)^{-1} > \tilde{r} > 0$, then the system exhibits a bistable behavior (phenotypic variability) for a range of values of $\tilde{a}$. Here we choose $n = 2$ and $\tilde{r} = 0.12$ such that there is a bistable region as in the case of the QS switch. The points (x_0, a_0) that define the bistable region correspond to the solutions of the polynomial equations [58],

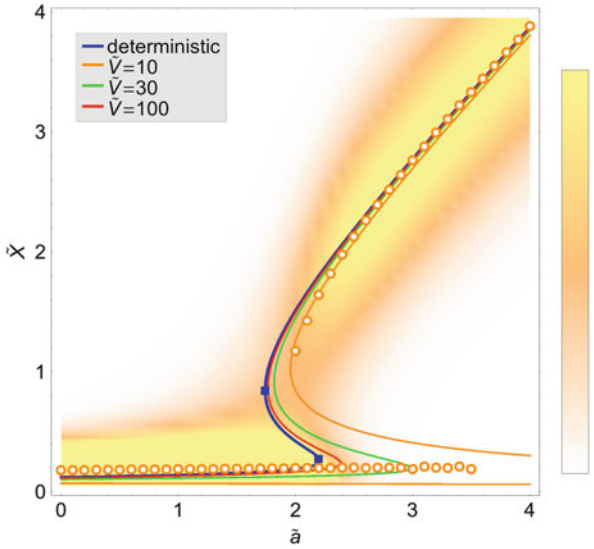

Fig. 3.12 Bifurcation diagram (phenotypic landscape) of the genetic auto-activating switch model. Bifurcation diagram of the autoactivating switch under deterministic (*blue line*) and stochastic conditions: *red, green, and orange lines* stand for the analytical location of the probability extrema for different noise intensities (see legend). The *open circles* indicate the results of numerical simulations of the case $\tilde{V} = 10$. The probability density of that case is also depicted by means of a density plot (logarithmic scale). The bistable region of the deterministic system gets delimited by the points (x_0, a_0) (*squares*). Note that noise stabilizes the low state and the bistable region expands

$$0 = \tilde{r} + \frac{\tilde{a}_0 \tilde{x}_0^2}{1 + \tilde{x}_0^2} - \tilde{x}_0 \tag{3.45}$$

$$0 = \frac{2\tilde{a}_0 \tilde{x}_0}{(1 + \tilde{x}_0^2)^2} - 1. \tag{3.46}$$

Figure 3.12 shows the stationary solution, $\tilde{x}_{\mathrm{st}}$, as a function of $\tilde{a}$ where set of points (x_0, a_0) are highlighted. Note that this bifurcation diagram reflects a situation akin to that of the QS switch.

If we now consider the biochemical fluctuations, the stochastic description of the system reads [16, 59]

$$\dot{\tilde{x}} = \tilde{r} + \tilde{a}\frac{\tilde{x}^2}{1 + \tilde{x}^2} - \tilde{x} + \xi(t)\sqrt{\tilde{r} + \tilde{a}\frac{\tilde{x}^2}{1 + \tilde{x}^2} + \tilde{x}} \tag{3.47}$$

where the noise term must be interpreted according to Itō and the statistical properties of the fluctuations are

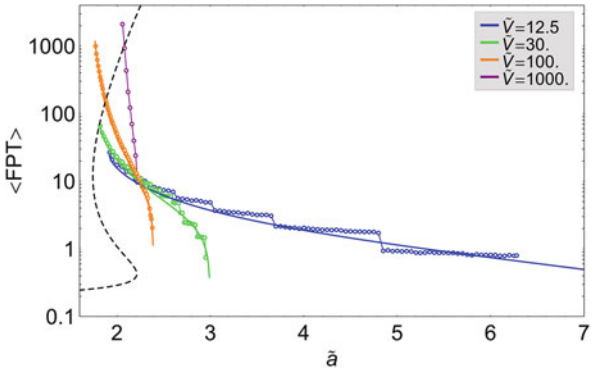

Fig. 3.13 First passage time and switching rate for the genetic switch. Mean first passage time (MFPT) for the genetic switch from the low stable state to the high state for different volume sizes, i.e. noise intensities (see legend). The *solid lines* correspond to the analytical solution and the *circles* to the Gillespie simulations. The deterministic bifurcation curve (*dashed line*) is depicted with an arbitrary y-scale in order to visualize the deterministic bistable region. Depending on the value of $\tilde{a}$, the MFPT increases or decreases with the intrinsic noise intensity

$$\langle \xi(t) \rangle = 0 \tag{3.48}$$

$$\langle \xi(t)\xi(t') \rangle = \tilde{\sigma}^2 \delta\left(t - t'\right). \tag{3.49}$$

In this case, the intensity of the fluctuations is related with the cellular volume such that $\tilde{\sigma}^2 = 1/\tilde{V}$, where $\tilde{V} = V \sqrt[n]{K_d}$ is the dimensionless volume.

Interestingly, the location of the bifurcation points that define the bistable region gets modified by the noise such that the low protein concentration state becomes more stable. An effect referred to as the *stochastic stabilization* of a phenotypic state [58]. Figure 3.12 shows this effect and reveals that the low state extends its stability with respect to the deterministic system.

The FPT statistics is related to the structure of the bifurcation diagram since the former evaluates the amount of time required to jump to a stable state. Thus, Fig. 3.13 shows the MFPT as a function of the control parameter $\tilde{a}$ for different volumes, namely noise intensities. We can observe the same counterintuitive behavior reported on the QS switch: depending on the value of $\tilde{a}$ (equivalent to the concentration of autoinducer in the QS switch), the MFPT increases or decreases with the intrinsic noise intensity. This effect can be now easily explained in terms of the modification of the bifurcation diagram due to noise that extends the stability of the low state. Up to the value of the control parameter where there is the bifurcation point of the deterministic system, the fluctuations help cells to jump to the high state. Beyond that point, the deterministic system "immediately" jumps. However, the stochastic system gets "trapped" in the low state. This causes the FPT to increase with respect to the deterministic situation such that the larger the noise the larger the FPT since the low state becomes more stable. In the context of the QS switch these results reveal that LuxR noise controls the precision by modifying

the phenotypic landscape and at the same time raises the following question: how comes LuxI noise has no effect on the QS phenotypic landscape? Note that LuxI fluctuations are transmitted to the autoinducer at the end. Yet, the diffusion process effectively averages out the fluctuations of the signaling molecule (see Sect. 3.2.5). That is, the effective cellular volume "perceived" by LuxI is the total volume of the cells. This is not possible for LuxR which is not driven by diffusion and is kept within the cell. As a result, the activation complex is susceptible to the fluctuations of LuxR but not to those of LuxI.

3.4 Discussion

In this chapter we have reviewed some studies that reveal the importance of stochasticity in QS. We first explored the role played by cell–cell communication and transcriptional noise in QS systems near the activation threshold where *luxI* is expressed at a low constitutive level such that the feedback regulation (autoactivation) can be disregarded. Under these conditions we have shown that the interplay between the diffusion and the mRNA dynamics plays a crucial role for regulating the total amount of noise. Thus, transcriptional noise is the main contribution to the total noise for a large range of diffusion values and only for large values of the diffusion the intrinsic noise is the major source of stochasticity. Importantly, we have shown that the total noise shows a non-monotonic behavior as a function of the diffusion rate that indicates a mechanism to reduce the signal to noise ratio.

Herein we have also introduced the concept of precision in the QS switch: a meaningful measure of the synchronization of the cells based on the *homogeneity* of the collective cell response. A small precision means a bimodal response over a broad range of autoinducer concentrations, producing a graded response at the population level. A high precision means a response that is mainly monomodal and a bimodal response over a narrow range of autoinducer concentrations, providing a steep response at the population level. The precision is highly dynamic and critically depends on the induction time and, importantly, on the noise levels of LuxR that influences the probability of a cell to jump from the deactivated to the activated state (change of phenotype). In addition, we have revealed that the noise at the level of LuxI does not modify the phenotypic landscape and consequently has no effect on the precision of the QS switch.

Interestingly, recent experiments have revealed the presence of additional regulatory interactions for controlling the LuxR noise levels. For example, C8HSL molecules, a secondary QS signal in *V. fischeri*, has been suggested to reduce the noise in bioluminescence output of the cells at low autoinducer concentrations [42]. In the same direction, in *V. harveyi*, the number of LuxR dimers is tightly regulated indicating a control over LuxR intrinsic noise [44]. In fact, wild-type *V. harveyi* strains have two negative feedback loops that repress the production of LuxR [60] and this kind of regulatory circuit is known to reduce noise levels [61]. In this context, the results reviewed here provide a feasible explanation for the network

structure in wild-type strains: since noise in LuxR controls the phenotypic variability of LuxR/LuxI QS systems, bacteria may have evolved mechanisms to control its noise levels. An additional argument in this regard arises from the simulation results about the deactivation process: once cells are fully induced the reversibility of the phenotype is a pretty rare event (FPT larger than 100 h). Thus, it makes sense that wild-type strains have additional interactions that regulate negatively *luxR* [45–47]. Moreover, it indicates that synthetic strains as *lux01* and *lux02* may summarize most features of the wild-type operon during the activation process but they fail to capture aspects of the deactivation phenomenon.

In regards to the importance of non-stationary effects, most works assume steady conditions. However, we have shown that the time for reaching a steady state of cell response distribution is much larger than the duration of the cell cycle. This is in agreement with experimental results [43] as well as with another stochastic model of QS transition in *Agrobacterium tumefaciens* [62]. In our simulations, the population of cells needs $\sim$30 h to reach a steady-state when induced at 50 nM of autoinducer and that this time is even larger close to the critical concentration of activation [18]. In most laboratory experiments studying the QS transition, the typical experimental run or time of culture growth before measurement rarely exceeds 20 h [43,44,57,63, 64], after which the expression of genes is assumed to reach a steady-state. While a modeling approach is certainly a crude simplification of the real genetic network, the results suggest that special care should be taken about transient effects when studying the population-wide QS response. Indeed, bistable gene networks are often associated with slow response time compared to graded-response gene networks [65, 66].

While speculative, these results about the importance of non-stationary effects can be extrapolated to growing colonies where the cell density is not kept constant as in our simulations or in the experiments we reproduced [18,43]. A good supply of nutrients implies short induction times since the concentration of autoinducer will quickly grow (exponentially) as the population size does. According to our results, this fast growing condition decreases the precision of the switch and, consequently, promotes variability at the population level (see Fig. 3.14, fast growth line). In addition, the full collective activation of the system would require a large population size (i.e., more autoinducer).

On the other hand, if the colony grows in an environment poor in nutrients, the concentration will increase slowly and the system will have time to reach the steady-state response (see Fig. 3.14, slow growth line). In this case, the precision would increase, the variability would be diminished, and full activation would require smaller colony sizes. Most phenotypic changes induced by the QS mechanism refer to bacterial strategies for survival and/or colonization. In this context, these results suggest that both the QS activation threshold and the phenotypic variability might depend on the growth rate of the colony and, as a consequence, on the environmental conditions. This is in fact in agreement with recent studies that show that the collective response of a population of cells depends not only on the underlying genetic circuit and the environmental signals but also on the speed of variation of these signals [67].

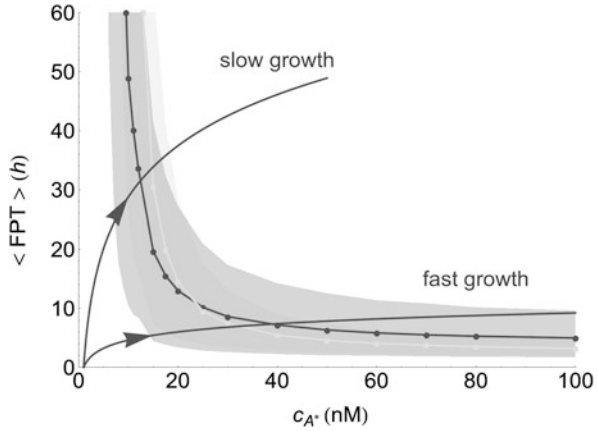

Fig. 3.14 The growth rate conditions the phenotypic variability. In the context of a growing colony, the autoinducer concentration increases as the colony does: *arrow lines* show schematically two exponential growth conditions for the autoinducer concentration as a function of time. Our results on the MFPT, valid at fixed autoinducer concentrations, can be extrapolated, qualitatively, to the case of increasing autoinducer levels. Fast growth results in a large cell variability and large critical colony size for achieving a global response, while slow growth produces reduced cell variability and a smaller critical population size. Increasing fluctuations in LuxR have two opposite effects: in the slow growth case, increasing the noise (*dark circles/shading*: $b_R = 20$; *light squares/shading*: $b_R = 0.01$) decreases the critical population size while hardly changing the variability, in the fast growth case, increasing noise increases the critical population size and increases greatly the variability

Finally, we have observed a counterintuitive effect of LuxR gene expression noise in the dynamics of the QS activation. For high concentration of autoinducer (above $\sim$25 nM) an increase in the noise intensity slows down the mean activation time. This effect is the opposite of what would be expected in the case of a bistable autoactivating switch with additive noise or extrinsic fluctuations [68]. In order to address this puzzling result, we have introduced a simple model that summarizes the underlying LuxR/LuxI motif: the autoactivating switch with a positive feedback loop. Thus, we have shown that intrinsic noise modifies the bifurcation diagram (phenotypic landscape) and stabilizes the low state of the cells; an effect that we call *stochastic stabilization*.

Our final comment refers to the possibility of considering other sources of stochasticity that may play a crucial role in QS. Cell-to-cell variability and extrinsic noise have been proved key in many cell processes [35, 49, 50, 69]. In the context of the problems studied herein, the results suggest that variability, either at the level of the mRNA dynamics or at the level of the diffusion rate, can effectively lead to significant changes in the reported phenomenology. However, theoretical studies [19, 70] suggest that the QS synchronization is robust to the variability in the diffusion rate and extracellular noise. Thus, whether or not these additional noise sources may generate new effects in the framework of QS is not clear yet

and further research is needed. In any case, stochasticity in QS is key for describing adequately the bacterial communication phenomena and therefore it is a promising field of research that will continue flourishing in next years.

References

1. Raj A, van Oudenaarden A (2008) Cell 135:216
2. Ullner E, Buceta J, Díez-Noguera A, García-Ojalvo J (2009) Biophys J 96:3573
3. Kaern M, Elston TC, Blake WJ, Collins JJ (2005) Nat Rev Genet 6:451
4. Eldar A, Elowitz MB (2010) Nature 467:167
5. Cai L, Dalal CK, Elowitz MB (2008) Nature 455:485
6. Pai A, You L (2009) Mol Syst Biol 5:286
7. Kaplan H, Greenberg E (1985) J Bacteriol 163:1210
8. Danino T, Mondragón-Palomino O, Tsimring L, Hasty J (2010) Nature 463(7279):326. DOI: 10.1038/nature08753
9. Tanouchi Y, Tu D, Kim J, You L (2008) PLoS Comput Biol 4:e1000167
10. Weber M, Buceta J (2011) BMC Syst Biol 5:11
11. Erdmann T, Howard M, ten Wolde PR (2009) Phys Rev Lett 103:2
12. Waters CM, Bassler BL (2005) Annu Rev Cell Dev Biol 21:319
13. Zhu XM, Yin L, Hood L, Ao P (2004) J Bioinformatics Comput Biol 2:785
14. Tian T, Burrage K (2006) PNAS 103:8372
15. Wang J, Zhang J, Yuan Z, Zhou T (2007) BMC Syst Biol 1:50
16. Frigola D, Casanellas L, Sancho JM, Ibañes M (2012) PLoS ONE 7:e31407
17. Kepler T, Elston T (2001) Biophys J 81:3116
18. Weber M, Buceta J (2013) BMC Syst Biol 7:6
19. Hong D, Saidel WM, Man S, Martin JV (2007) J Theor Biol 245:726
20. Yu J, Xiao J, Ren X, Lao K, Xie XS (2006) Science 311:1600
21. Choi PJ, Cai L, Frieda K, Xie XS (2009) Science 322:442
22. Horsthemke W, Lefever R (1984) Noise-induced transitions: theory and applications in physics, chemistry and biology. Springer, New York
23. More MI, Finger LD, Stryker JL, Fuqua C, Eberhard A, Winans SC (1996) Science 272:1655
24. Parsek MR, Val DL, Hanzelka BL, Cronan JE, Greenberg EP (1999) PNAS 96:4360
25. Shahrezaei V, Swain PS (2008) PNAS 105:17256
26. Kaufmann G, Sartorio R, Lee S, Rogers C, Meijler M, Moss J, Clapham B, Brogan A, Dickerson T, Janda K (2005) PNAS 102:309
27. Roberts C, Anderson KL, Murphy E, Projan SJ, Mounts W, Hurlburt B, Smeltzer M, Overbeek R, Disz T, Dunman PM (2006) J Bacteriol 188:2593
28. Anderson KL, Dunman PM (2009) Int J Microbiol 2009:525491
29. Pearson J, Van Delden C, Iglewski B (1999) J Bacteriol 181:1203
30. Xavier K, Bassler B (2005) J Bacteriol 187:238
31. Wang L, Hashimoto Y, Tsao C, Valdes J, Bentley W (2005) J Bacteriol 187:2066
32. Herzberg M, Kaye I, Peti W, Wood T (2006) J Bacteriol 188:587
33. Li J, Wang L, Hashimoto Y, Tsao CY, Wood TK, Valdes JJ, Zafiriou E, Bentley WE (2006) Mol Syst Biol 2:67
34. Gillespie D (1977) J Phys Chem 81:2340
35. Elowitz MB, Levine AJ, Siggia ED, Swain PS (2002) Science 297:1183
36. Swain P, Elowitz M, Siggia E (2002) PNAS 99:12795
37. Nealson K, Platt T, Hastings J (1970) J Bacteriol 104:313
38. Pérez PD, Hagen SJ (2010) PLoS ONE 5:e15473
39. Anetzberger C, Pirch T, Jung K (2009) Mol Microbiol 73:267

40. Boedicker JQ, Vincent ME, Ismagilov RF (2009) Angew Chemie 48:5908
41. Hagen SJ, Son M, Weiss JT, Young JH (2010) J Biol Phys 36:317
42. Pérez PD, Weiss JT, Hagen SJ (2011) BMC Syst Biol 5:153
43. Williams JW, Cui X, Levchenko A, Stevens AM (2008) Mol Syst Biol 4:234
44. Teng SW, Wang Y, Tu KC, Long T, Mehta P, Wingreen NS, Bassler BL, Ong NP (2010) Biophys J 98:2024
45. Lyell NL, Dunn AK, Bose JL, Stabb EV (2010) J Bacteriol 192:5103
46. Septer AN, Stabb EV (2012) PLoS ONE 7:e49590
47. Sitnikov D, Shadel G, Baldwin T (1996) Mol General Genet 252:622
48. Shadel G, Baldwin T (1992) J Biol Chem 267:7690
49. Canela-Xandri O, Sagués F, Buceta J (2010) Biophys J 98:2459
50. Rosenfeld N, Young JW, Alon U, Swain PS, Elowitz MB (2005) Science 307:1962
51. Urbanowski M, Lostroh C, Greenberg E (2004) J Bacteriol 186:631
52. Süel GM, Kulkarni RP, Dworkin J, García-Ojalvo J, Elowitz MB (2007) Science 315:1716
53. Cai L, Friedman N, Xie XS (2006) Nature 440:358
54. Ozbudak EM, Thattai M, Kurtser I, Grossman AD, van Oudenaarden A (2002) Nat Genet 31:69
55. Gardiner C (1985) Handbook of stochastic methods: for physics, chemistry and the natural sciences. Springer, New York
56. Isaacs FJ, Hasty J, Cantor CR, Collins JJ (2003) PNAS 100:7714
57. Ozbudak E, Thattai M, Lim H, Shraiman B, Van Oudenaarden A (2004) Nature 427:737
58. Weber M, Buceta J (2013) PLoS ONE 8:e73487
59. Gillespie D (2000) J Chem Phys 113:297
60. Tu KC, Long T, Svenningsen SL, Wingreen NS, Bassler BL (2010) Mol Cell 37:567
61. Balázsi G, van Oudenaarden A, Collins JJ (2011) Cell 144:910
62. Goryachev AB, Toh DJ, Wee KB, Zhang HB, Zhang LH, Lee T (2005) PLoS Comput Biol 1:e37
63. Long T, Tu KC, Wang Y, Mehta P, Ong NP, Bassler BL, Wingreen NS (2009) PLoS Biol 7:e68
64. Anetzberger C, Schell U, Jung K (2012) BMC Microbiol 12:209
65. Savageau Ma (2002) Math Biosci 180:237
66. Tiwari A, Ray JCJ, Narula J, Igoshin Oa (2011) Math Biosci 231:76
67. Nené NR, García-Ojalvo J, Zaikin A (2012) PLoS ONE 7:e32779
68. Zheng XD, Yang XQ, Tao Y (2011) PLoS ONE 6:e17104
69. Shahrezaei V, Ollivier J, Swain P (2008) Mol Syst Biol 4:196
70. Mina P, di Bernardo M, Savery NJ, Tsaneva-Atanasova K (2013) J Roy Soc Interface Roy Soc 10:20120612